

A Possible Bifurcation in Atmospheres of Strongly Irradiated Stars and Planets

Ivan Hubeny^{1,2}

Adam Burrows³ & David Sudarsky³

ABSTRACT

We show that under certain circumstances the differences between the absorption mean and Planck mean opacities can lead to multiple solutions for an LTE atmospheric structure. Since the absorption and Planck mean opacities are not expected to differ significantly in the usual case of radiative equilibrium, non-irradiated atmospheres, the most interesting situations where the effect may play a role are strongly irradiated stars and planets, and also possibly structures where there is a significant deposition of mechanical energy, such as stellar chromospheres and accretion disks. We have presented an illustrative example of a strongly irradiated giant planet where the bifurcation effect is predicted to occur for a certain range of distances from the star.

Subject headings: radiative transfer—stars: atmospheres, low-mass, brown dwarfs—planets and satellites: general—planetary systems: general—binaries: general

1. Introduction

There are many situations where the atmosphere of an object, a star or a planet, is irradiated by a companion star in such a way that this irradiation significantly influences its atmospheric structure. In the case of classical close binary stars, the effect exists, but is rarely dramatic because the effective temperatures differ by a factor of a few. On the other hand, the effect may be quite dramatic in the case of sub-stellar mass objects such as giant planets and brown dwarfs, irradiated by a solar-type star, in which case the ratio of their effective temperatures may reach a factor of 100 or more. We stress that we use the term

¹NOAO, P.O.Box 26732, 950 N. Cherry, Tucson, AZ 85726

²LASP, NASA Goddard Space Flight Center, Greenbelt, MD 20771

³Department of Astronomy and Steward Observatory, The University of Arizona, Tucson, AZ 85721

effective temperature as used in the theory of stellar atmospheres, namely as a measure of the total energy flux coming from the interior of the object.

In the case of extrasolar giant planets (EGP), we recently have witnessed a significant increase in interest in predicting EGP spectra. This was motivated in part by two detected planetary transits, which are in principle able to provide direct information about the planet's atmosphere. Another motivation is the need to predict spectra of extrasolar planets to guide the design of future missions which aim at recording EGP spectra .

We have recently computed a large set of model atmospheres and spectra of EGPs (Sudarsky, Burrows, & Hubeny 2003 - hereafter referred to as SBH). We have used a modification of our universal stellar atmosphere program TLUSTY (Hubeny 1988; Hubeny & Lanz 1995), called COOLTLUSTY. This variant does not compute opacities on the fly; instead it uses a pretabulated opacity as a function of wavelength, temperature, and density. The tables are computed using an updated version of the chemical equilibrium code of Burrows & Sharp (1999), which includes a prescription to account for the rainout of species in a gravitational field.

Motivated by the recent discovery of the second transiting planet OGLE-TR-56 (Konacki et al. 2003; Sasselov 2003), which is believed to have a separation of a mere 0.0225 AU from its parent star, we tried to extend the SBH models to higher irradiations. However, COOLTLUSTY faced significant convergence problems. After various attempts and using various strategies, we have discovered that the convergence behavior is not the result of a bug in the program, or of an insufficiency in our numerical scheme, but is in fact a consequence of an existence of multiple solutions that may lead to disastrous effects for convergence. When studying the effect, we found that its roots are quite general, and are in fact applicable to other cases in the theory of stellar atmospheres. Therefore, we devote the present paper to explain the effect in general terms.

2. Basic Equations

The atmospheric structure is obtained by solving simultaneously the radiative transfer equation, the radiative equilibrium equation, and the hydrostatic equilibrium equation. For simplicity, we assume LTE. Since our basic aim here is to study atmospheres of irradiated giant planets, this approximation is a reasonable one, although it should be relaxed in the future, as was the LTE assumption eventually relaxed in modern studies of stellar atmospheres. Here, we present a brief overview of the basic equations.

The radiative transfer equation is written as

$$\mu \frac{dI_{\nu\mu}}{dm} = \chi_{\nu} (I_{\nu\mu} - S_{\nu}) , \quad (1)$$

where $I_{\nu\mu}$ is the specific intensity of radiation as a function of frequency, ν , angle - described through the cosine of the angle of propagation with respect to the normal to the surface, μ , and the geometrical coordinate, taken here as the column mass m . The later is defined as $dm = -\rho dz$, where z is a geometrical distance (measured outwards), and ρ the mass density. The monochromatic optical depth is defined as $d\tau_{\nu} = \chi_{\nu} dm$. Finally, S_{ν} is the source function, given in LTE by

$$S_{\nu} = \frac{\kappa_{\nu}}{\chi_{\nu}} B_{\nu} + \frac{\sigma_{\nu}}{\chi_{\nu}} J_{\nu} . \quad (2)$$

Here, κ_{ν} is the true absorption coefficient, σ_{ν} the scattering coefficient, and $\chi_{\nu} = \kappa_{\nu} + \sigma_{\nu}$ is the total extinction coefficient. All coefficients are per unit mass.

The boundary conditions are provided through the diffusion approximation at the deepest point,

$$I_{\nu\mu}(\tau_{\max}) = B_{\nu}(T(\tau_{\max})) + \mu \frac{dB_{\nu}}{d\tau_{\nu}} \Big|_{\tau_{\max}} , \quad \mu > 0 , \quad (3)$$

and the upper boundary condition is

$$I_{\nu\mu}(0) = I_{\nu\mu}^{\text{ext}} , \quad \mu < 0 , \quad (4)$$

where $I_{\nu\mu}^{\text{ext}}$ is the specific intensity of the external irradiation. For simplicity, we assume isotropic irradiation, $I_{\nu\mu}^{\text{ext}} = J_{\nu}^{\text{ext}}$. It is convenient to express the frequency-integrated irradiation intensity as

$$J^{\text{ext}} \equiv \int_0^{\infty} J_{\nu}^{\text{ext}} d\nu = WB(T_{*}) , \quad (5)$$

where T_{*} is an effective temperature of the irradiating star (in case the irradiation source is not a star, T_{*} is merely the characteristic temperature of the incoming radiation), and W a dilution factor.

The moments of the specific intensity are defined as

$$[J_{\nu}, H_{\nu}, K_{\nu}] \equiv (1/2) \int_{-1}^1 I_{\nu\mu} [1, \mu, \mu^2] d\mu . \quad (6)$$

The first moment of the transfer equation is written

$$\frac{dH_{\nu}}{dm} = \chi_{\nu} (J_{\nu} - S_{\nu}) = \kappa_{\nu} (J_{\nu} - B_{\nu}) , \quad (7)$$

where the second equality follows from equation (2). Integrating over frequency we obtain

$$\frac{dH}{dm} = \kappa_J J - \kappa_B B, \quad (8)$$

where κ_J and κ_B are the absorption and Planck mean opacities, respectively, defined by

$$\kappa_J = \frac{\int_0^\infty \kappa_\nu J_\nu d\nu}{\int_0^\infty J_\nu d\nu}, \quad (9)$$

and

$$\kappa_B = \frac{\int_0^\infty \kappa_\nu B_\nu d\nu}{\int_0^\infty B_\nu d\nu}. \quad (10)$$

These two opacities are usually assumed to be equal. This is an excellent approximation in the case of non-irradiated atmospheres, because $J_\nu \approx B_\nu$ in optically thick regions, and $J_\nu(\tau < 1) \propto (1/2)B_\nu(\tau = 1)$ (the Eddington-Barbier relation), so J is proportional to B and the averaging over J and B leads to very similar results. However, here we maintain the distinction because the difference between κ_J and κ_B turns out to be crucial in the case of strongly irradiated atmospheres.

The second moment of the transfer equation is

$$\frac{dK_\nu}{dm} = \chi_\nu H_\nu, \quad (11)$$

and integrating over frequency we obtain

$$\frac{dK}{dm} = \chi_H H, \quad (12)$$

where

$$\chi_H = \frac{\int_0^\infty \chi_\nu H_\nu d\nu}{\int_0^\infty H_\nu d\nu}, \quad (13)$$

which is called the flux mean opacity. Notice that unlike the two previous opacities, which were averages of the *true* absorption coefficient (without the scattering term), the flux-mean opacity contains the *total* absorption coefficient.

Finally, the radiative equilibrium equation is written

$$\int_0^\infty \kappa_\nu (J_\nu - B_\nu) d\nu = 0, \quad (14)$$

which can be rewritten, using the above defined mean opacities, as

$$\kappa_J J - \kappa_B B = 0. \quad (15)$$

Substituting (15) into (8), we obtain another form of the radiative equilibrium equation:

$$\frac{dH}{dm} = 0, \quad \text{or} \quad H = \text{const} \equiv (\sigma/4\pi) T_{\text{eff}}^4, \quad (16)$$

where σ is the Stefan-Boltzmann constant.

3. Temperature Structure

3.1. General

The above equations are *exact*, given LTE, but are of course only formal because the mean opacities κ_J and χ_H are not known in advance; only κ_B is a known function of temperature and density. Nevertheless, assuming that they are known and equal to the Rosseland mean opacity, we may write a solution for temperature, following the classical textbook procedure, known by the name of “LTE-grey model atmospheres” (e.g. Mihalas 1978). A generalization of a classical model for the case of external irradiation is given by Hummer (1982), and for the case of accretion disks and unequal mean opacities by Hubeny (1990).

The procedure is as follows. From equation (15) we have $B = (\kappa_J/\kappa_B)J$, which allows us to express T through J using the well-known relation $B = (\sigma/\pi)T^4$. To determine J , we use the solution for the second moment of the transfer equation $K(\tau_H) = H\tau_H + K(0) = (\sigma/4\pi)T_{\text{eff}}^4\tau_H + K(0)$, where τ_H is the optical depth associated with the flux-mean opacity, and express the moment K in terms J using the Eddington factor, $f_K \equiv K/J$. Similarly, we express the surface flux through the second Eddington factor, $f_H \equiv H(0)/J(0)$, and we end up with (see also Hubeny 1990)

$$T^4 = \frac{3}{4} T_{\text{eff}}^4 \frac{\kappa_J}{\kappa_B} \left[\frac{1}{3f_K} \tau_H + \frac{1}{3f_H} \right] + \frac{\kappa_J}{\kappa_B} W T_*^4. \quad (17)$$

Again, this solution is exact within LTE. The usual LTE-grey model consists in assuming that all the mean opacities are equal to the Rosseland mean opacity. Moreover, if one adopts the Eddington approximation ($f_K = 1/3$; $f_H = 1/\sqrt{3}$), then one obtains a simple expression

$$T^4 = \frac{3}{4} T_{\text{eff}}^4 \left(\tau + 1/\sqrt{3} \right) + W T_*^4. \quad (18)$$

We will consider the most interesting case, namely that of strong irradiation, defined by $W T_*^4 \gg T_{\text{eff}}^4$. In this case, the second term in brackets is negligible, and we may define a *penetration depth* as the optical depth where the usual thermal part ($\propto T_{\text{eff}}^4$) and the irradiation part ($\propto W T_*^4$) are nearly equal, viz.

$$\tau_{\text{pen}} \approx W \left(\frac{T_*}{T_{\text{eff}}} \right)^4. \quad (19)$$

The behavior of the local temperature in the case of the strictly gray model is very simple – it is essentially constant, $T = T_0 \equiv W^{1/4} T_*$ for $\tau < \tau_{\text{pen}}$, and follows the usual distribution $T \propto \tau^{1/4} T_{\text{eff}}$ in deep layers, $\tau > \tau_{\text{pen}}$. We stress that while the strictly gray model exhibits an essentially isothermal structure down to $\tau \approx \tau_{\text{pen}}$, such will not be the case for a nongray model, as we shall show in detail in the next sections.

3.2. Surface Layers

In the general case, we have to retain the ratio of the absorption and Planck mean opacities. In the irradiation-dominated layers ($\tau_H < \tau_{\text{pen}}$), the temperature is given by

$$T = \gamma W^{1/4} T_*, \quad (20)$$

where

$$\gamma \equiv (\kappa_J / \kappa_B)^{1/4}. \quad (21)$$

As stated before, $\gamma \approx 1$ in the case of no or weakly irradiated atmospheres. However, in the case of strong irradiation, γ may differ significantly from unity, and, moreover, may be a strong function of temperature, and to a lesser extent density. This is easily seen by noticing that in optically thin regions, the local mean intensity is essentially equal to twice the irradiation intensity, because the incoming intensity is equal to the irradiation intensity, and the outgoing intensity is roughly equal to it as well. The reason is that in order to conserve the total flux when it is much smaller than the partial flux in the inward or the outward direction, both fluxes should be almost equal, as are the individual specific and mean intensities. More specifically,

$$H = H^{\text{out}} - H^{\text{ext}} = \int_0^\infty \int_0^1 I_{\nu\mu} \mu d\mu d\nu - \int_0^\infty \int_0^1 I_{\nu,-\mu} \mu d\mu d\nu. \quad (22)$$

If $H \ll H^{\text{ext}}$, then we must have $\int_0^\infty I_{\nu\mu} d\nu \approx \int_0^\infty I_{\nu,-\mu} d\nu$ for all angles, and thus $J_\nu \approx 2J_\nu^{\text{ext}} \approx 2W^{1/4}B_\nu(T_*)$. We may then write the absorption mean opacity as a function of T and T_* as

$$\kappa_J(T, T_*) \approx \frac{\int \kappa_\nu(T) W B_\nu(T_*) d\nu}{\int W B_\nu(T_*) d\nu} = \frac{\int \kappa_\nu(T) B_\nu(T_*) d\nu}{\int B_\nu(T_*) d\nu}. \quad (23)$$

The dilution factor cancels out, and only the spectral distribution of the irradiation intensity matters.

In other words, the absorption mean is an average of the opacity weighted by the Planck function corresponding to the effective temperature of the source of irradiation, while the Planck mean is an average of the opacity weighted by the Planck function corresponding to the *local* temperature. Obviously, they can be quite different. If the monochromatic opacity differs significantly in the region where $B_\nu(T)$ and $B_\nu(T_*)$ have their local maxima, the resulting κ_J and κ_B will differ substantially. If, moreover, and this is the crucial point, the monochromatic opacity depends sensitively on temperature, the opacity ratio γ may have a complex, and generally non-monotonic, dependence on temperature.

The local temperature in the upper layers is given, in view of equation (20), by the expression

$$T/T_0 = \gamma(T). \quad (24)$$

It is now clear that if γ exhibits a strongly non-monotonic behavior in the vicinity of T_0 , for instance if it has a pronounced minimum or maximum there, equation (24) may have *two or even more solutions!*

3.3. Deep Layers

The bifurcation behavior is not limited to the surface layers, but may continue to large optical depths. This might seem surprising at first sight because from Equation (17) one may expect that once $\tau > 1$, the mean opacities κ_J and κ_B become roughly equal, and the Eddington factor is $f_K \approx 1/3$, so that $T = T_0$ all the way till τ_{pen} . We recall that the penetration depth may be quite large; for instance for the case $T_{\text{eff}} = 75$ K, $T_* = 6000$ K, and $W = 2.2 \times 10^{-3}$ (the case studied in detail in the next Section), $\tau_{\text{pen}} = 9 \times 10^4$.

However, the behavior of the local temperature may be more complicated. This is linked to another interesting inequality of mean opacities that is usually taken for granted, namely the flux mean opacity χ_H and the Rosseland mean opacity χ_{ross} . The Rosseland mean opacity is in fact defined in such a way that it is equal to the flux mean opacity in the diffusion approximation. Indeed, in this approximation,

$$H_\nu \approx \frac{1}{3} \frac{dB_\nu}{d\tau_\nu} = \frac{1}{3} \frac{1}{\chi_\nu} \frac{dB_\nu}{dm} = \frac{1}{3} \frac{1}{\chi_\nu} \frac{dB_\nu}{dT} \frac{dT}{dm},$$

and therefore

$$\chi_H \approx \frac{\int_0^\infty \frac{dB_\nu}{dT} d\nu}{\int_0^\infty \frac{1}{\chi_\nu} \frac{dB_\nu}{dT} d\nu} \equiv \chi_{\text{ross}},$$

where the latter equality represents the definition of the Rosseland mean opacity.

In the case of strong irradiation, an interesting, and fundamentally different, situation appears. Since the net flux is very small, the total flux in the $\mu > 0$ (outgoing) hemisphere is roughly equal to that in the $\mu < 0$ (incoming) hemisphere (see above). Because the monochromatic opacity varies strongly with frequency, there are frequency regions where the net monochromatic flux is positive, and regions where it is negative. The flux-mean opacity close to the surface may attain large values, either positive or negative, depending upon whether χ_ν weighs the positive or negative net flux regions more.

Going to deeper layers, the net monochromatic flux decreases because the radiation field becomes more isotropic for all frequencies, so that the flux mean opacity decreases. Consequently, the corresponding flux-mean optical depth increments $\Delta\tau_H \approx \chi_H \Delta m$ become very small, and τ_H will exhibit a plateau where it remains essentially constant with m . Finally, in the regions where all the influence of the external irradiation dies out, the usual

diffusion approximation sets in, and the flux-mean optical depth becomes essentially equal to the Rosseland optical depth.

This means that for strong irradiation, the temperature in the deep layers should exhibit a plateau with

$$T_{\text{plateau}} \approx \frac{3}{4} T_{\text{eff}}^4 \bar{\tau}_H, \quad (25)$$

where $\bar{\tau}_H$ is the plateau value of the flux-mean optical depth. The value of $\bar{\tau}_H$ and thus T_{plateau} depends upon the exact form of the monochromatic opacity; a rough estimate is provided by setting $\bar{\tau}_H \approx \tau_{\text{pen}}$, in which case $T_{\text{plateau}} \approx (7/4)^{1/4} W^{1/4} T_* \approx 1.15 T_0$.

4. Example of an Extrasolar Giant Planet Irradiated by a Solar-type Star

4.1. Opacities

Using partition functions, LTE level densities, stimulated emission corrections, and broadening algorithms, we generated opacity tables from numerous available line lists. For gaseous H₂O, Partridge and Schwenke (1997) have calculated the strengths of more than 3×10^8 lines. We used a subset of their 4×10^7 strongest lines. For various other molecular species (*e.g.*, NH₃, PH₃, H₂S and CO), we used the HITRAN (Rothman *et al.* 1992,1998) and GEISA (Husson *et al.* 1994) databases, augmented with additional lines from theoretical calculations and measurements (Tyuterev *et al.* 1994; Goorvitch 1994; Tipping 1990; Wattson and Rothman 1992). For methane, shortward of $\sim 1.0 \mu\text{m}$ we used the Karkoschka (1994) opacities and between $\sim 1.0 \mu\text{m}$ and $1.58 \mu\text{m}$ we used the Strong *et al.* (1993) opacities. Longward of $1.58 \mu\text{m}$, we used the Dijon methane database (Borysow *et al.* 2003) that includes the hot bands. Opacity due to Collision-Induced Absorption (CIA) by H₂ and helium is taken from Borysow and Frommhold (1990), Zheng and Borysow (1995), and Borysow, Jørgensen, and Zheng (1997), as updated in Borysow (2002).

FeH and CrH opacities were taken from Dulick *et al.* (2003) and Burrows *et al.* (2002), respectively. The TiO line lists for its nine major electronic systems were taken from the Schwenke *ab initio* calculations, as modified by Allard, Hauschildt, and Schwenke (2000). These data include lines due to isotopically substituted molecules ⁴⁶Ti¹⁶O, ⁴⁷Ti¹⁶O, ⁴⁹Ti¹⁶O and ⁵⁰Ti¹⁶O relative to the most abundant isotopic form ⁴⁸Ti¹⁶O. For VO, we used the line list provided by Plez (1999). Because ⁵¹V is by far vanadium’s most abundant isotope, the lines of isotopically substituted molecules are not necessary. The line lists and strengths for the neutral alkali elements (Li, Na, K, Rb and Cs) were obtained from the Vienna Atomic Line Data Base (Piskunov *et al.* 1995). The general line shape theory of Burrows, Marley, and Sharp (2000) was used for Na and K, while those of Nefedov *et al.* (1999) and Dimitrijević

and Peach (1990) were used for the other alkali metals.

In practice, we pre-calculate a large opacity table in T/ρ /frequency space in which we interpolate during the iteration of the atmosphere/spectral model to convergence. The table contains 30,000 frequency points from 0.3 to 300 μm , uniformly spaced in steps of 1 cm^{-1} . Generally, 5000 geometrically-spaced frequency points are used in the radiative transfer model. In other words, our approach belongs to the category of “opacity sampling” methods for treating line blanketing.

We consider two different opacity tables; one which includes opacity due to TiO and VO, and the other one without these molecules. In the case without TiO/VO, these species were removed both from the opacity table as well as from the state equation, so these species are considered as completely absent everywhere in the atmosphere. These two different opacity tables suggest themselves because for an irradiated atmosphere we obtain high temperatures in the low pressure outer atmosphere. Importantly, temperature inversions are very possible. However, thermochemical equilibrium calculations with rainout (Burrows & Sharp 1999; Lodders & Fegley 2002) suggest that TiO and VO would exist at such high- T /low- P points. Since the presence of TiO and VO is quite natural at high- T /high- P points, one confronts a situation in which there are two regions rich in TiO/VO, separated by a middle region that is TiO/VO free. In a gravitational field with a monotonic pressure profile, this gap could act like a cold trap in which the TiO/VO that is transported by molecular or eddy diffusion from the upper low- P region into the intermediate cooler region, would condense and settle out, thereby depleting the upper low- P TiO/VO-rich region. This would eventually leave no TiO/VO at altitude to provide the significant absorption that could lead to a bifurcation. However, the cold-trap effect can not be anticipated in abundance tables that are functions of temperature and pressure alone. These tables are not cognizant of gravity, nor are they aware of the global T/P profile. Whether this cold-trap effect in fact happens is not yet clear. Furthermore, the same cold-trap effect might obtain for other EGP species (e.g. Fe). Hence, we use the presence or absence of TiO/VO at high- T /low- P points and the associated ambiguity as a means to explore the real mathematical bifurcation effect we have identified in this paper and leave to a future work the study of the true viability of cold traps in irradiated EGP atmospheres.

4.2. Results

We consider an intrinsically cold giant planet, with $T_{\text{eff}} = 75$ K, $\log g = 3$, irradiated by a G0V star with a spectral energy distribution taken for simplicity to be the corresponding Kurucz (1994) model atmosphere. We consider the class V, “roaster” situation, as defined

by SBH.

The opacity ratio index γ is plotted in Figure 1 as a function of temperature, for three densities characteristic to the outer layers of an atmosphere – $\rho = 10^{-12}$, 10^{-11} , and 10^{-10} g cm $^{-3}$. The upper panel shows the results for the opacities including TiO/VO, while the lower panel shows those without TiO/VO. It is clearly seen that in the former case the ratio κ_J/κ_B , and thus γ , exhibits a sharp peak around 1500 K; the dependence on density is not strong. The ratios T/T_0 for $T_0 = 450$ K (weak irradiation), 1250 K (medium strong irradiation), and 2600 K (very strong irradiation) are overplotted with dotted lines. The latter roughly corresponds to the case of the recently discovered transiting planet OGLE-TR-56. According to equation (24), the temperature at the surface layers is found at the intersection of the curves of $\gamma(T)$ and T/T_0 ; thus, we see that for low and for high irradiation there are unique solutions (corresponding to $T \approx 250$ K and $T \approx 2600 - 3000$ K, but that in the intermediate cases there are indeed multiple solutions.

The opacity table without TiO/VO does not exhibit a peak around 1500 K, and as it is clearly seen from the lower panel of Fig. 1, one obtains unique solutions for the temperature for all reasonable irradiations. Mathematically, the case of truly extreme irradiation (e.g. with T_0 around 4700 K) might again lead to multiple solutions⁴ because the line T/T_0 now almost coincides with $\gamma(T)$. However, we do not consider such a case here because then a host of new phenomena which we do not address in our present model, such as departures from LTE, dynamical effects, etc., would likely become crucial.

To explain the behavior of the κ_J over κ_B ratio, we plot in Figure 2 two examples of the monochromatic opacity, for $T = 1600$ K (close to the maximum of γ), and $T = 520$ K (the region near the minimum of γ). In both cases $\rho = 10^{-11}$ g cm $^{-3}$. We also plot normalized Planck functions for the two nominal temperatures, 1600 and 520 K (dotted lines), and for $T = T_* = 6000$ K (dashed line). The latter weighs most heavily the optical region around $\nu \approx 4 - 5 \times 10^{14}$ Hz, while the local Planck functions put the weight at much lower frequencies (around 10^{14} and 3×10^{13} Hz, respectively). In the case of the higher temperature, $T = 1600$ K, the monochromatic opacity exhibits a maximum just in the region where the Planck function corresponding to T_* is largest (because of TiO and VO); therefore, $\kappa_J > \kappa_B$. For the lower temperature, $T = 520$ K, the opacity in the optical range is lower by orders of magnitude, so κ_J is now significantly lower. Since the Planck function for $T = 520$ K emphasizes frequencies below 7×10^{13} Hz, where the monochromatic opacity is very large, we obtain $\kappa_J < \kappa_B$.

There are two other features seen in Figure 2 that are worth noticing. First, there is

⁴We are indebted to the referee for pointing out this possibility to us.

a large increase of γ for temperatures around and below 100 K. This is a consequence of low opacity at low frequencies. However, the opacity sources are quite uncertain in this regime. For studies of extremely cool objects the opacity table should be checked and possibly upgraded, but studying these objects is not our objective here. Second, in the case of no TiO/VO opacity (lower panel), it appears that γ nearly coincides with T/T_* . Taken at the face value, this would imply that the ratio $\int \kappa_\nu B_\nu(T_*) d\nu / \int \kappa_\nu B_\nu(T) d\nu$ is very close to unity.⁵ However, we do not see any compelling reason why this should be generally valid, so we conclude that such a behavior is just a coincidence.

In Figure 3 we demonstrate the behavior of the flux-mean opacity discussed in §3.3. The high-surface- T branch exhibits a negative flux mean optical depth at the surface layers because the opacity is high in the optical region where the next flux is negative. Consequently, the flux-mean opacity is negative there, and thus the flux-mean opacity (and the corresponding optical depth) on the plateau is lower than in the case of the low-surface- T branch.

We have also computed exact LTE models as described in SBH. We have used the stellar atmosphere code COOLTLUSTY, which is a variant of the universal program TLUSTY (Hubeny 1988; Hubeny & Lanz 1995). We stress that the emergent flux is not computed by a separate program; instead it is computed already by COOLTLUSTY. This also means that we do not use different opacity tables for computing the atmospheric structure and for computing the spectra. We have also tested the sensitivity of the computed model on different opacity samplings; we have resampled our original frequency grid of 5000 points to lower numbers of frequencies, and even for 300 points we found very little differences in the temperature structure (of the order of a few K). In some cases it was found advantageous to converge first a model with 300 frequencies, and using this as an input to reconverge a model with the full grid of 5000 frequencies in the next step.

The temperature structure is displayed in Figure 4, which demonstrates that the simplified description put forward above faithfully reflects the true behavior of temperature. Full lines represent models computed for the opacity table without TiO/VO, while the dashed and dot-dashed lines represent models with TiO/VO. The models without TiO/VO always converged to a unique solution, moreover with temperature monotonically decreasing outward, as we may have expected from the above discussion.

The behavior of the models with TiO/VO is more interesting. The high-irradiation model, the top dashed line, indeed converged to a unique solution. The surface temperature is 2600 K, in excellent agreement with the value expected from Figure 1 (the density at the

⁵We are indebted to the referee for drawing our attention to this point.

uppermost point is about $3 \times 10^{-12} \text{ g cm}^{-3}$). Even the initial increase of temperature in the upper layers when going inward is explained by Figure 1, since for progressively higher densities the solution of $T/T_0 = \gamma(T)$ occurs at higher temperatures. The low-surface- T solution is very close to the no-TiO/VO model, which once again demonstrates that the bifurcation is caused by the TiO/VO opacity. We have also examined depth-dependent concentrations of TiO and VO. Indeed, the mole fraction of TiO drops precipitously from $\approx 3 \times 10^{-7}$ to essentially zero at $m \approx 1.6 \times 10^{-2} \text{ g cm}^{-3}$ (that is at pressure $\approx 1.6 \times 10^{-5}$ bars and temperature $T \approx 1500 \text{ K}$) for the high-surface- T model; while it is not present in the low-surface- T model. Behavior of the VO concentration is analogous.

The low-irradiation model also converged to a unique solution; moreover, its surface temperature of about 250 K is in excellent agreement with the value one may expect from Figure 1. Again, both models, without and with TiO/VO agree very well.

The two middle curves, the dashed and dot-dashed curves, correspond to the same irradiation, and, thus, represent the bifurcation predicted by our analysis. The model with high surface temperature was converged starting from the extremely irradiated model (through several intermediate steps), while the model with the low surface temperature was converged starting from scratch, i.e. from a usual LTE-gray model in which all mean opacities are created equal. The high surface temperature at about 2200 K essentially coincides with the high-temperature intersection of about 2200 K on Figure 1. The low-surface- T solution exhibits a somewhat higher temperature than would follow from the low- T intersection in Figure 1 – 650 versus 550 K, but in view of all the approximations involved such an agreement is still very good. We did not numerically find the third possible solution with a surface T of about 1300 - 1400 K.

We stress that the numerical solutions were not contrived in any way to lead to the predicted bifurcation. In fact, we first discovered the effect purely numerically – we obtained two different, yet perfectly well converged solutions, depending on the input model. We have continued the convergence of both solution until the maximum relative change of temperature and density decreased below 10^{-5} in all depth points.

Several features of the overall accuracy of the model are worth mentioning. In fact, the low value of maximum relative change of temperature and density is not a satisfactory criterion of the convergence. One should also check the accuracy of the computed flux gradient and the value of the net flux. That is, for the former case we have to examine the quantity $e_{\text{grad}} = (\kappa_J J - \kappa_B B) / \kappa_B B$, and for the latter case the quantity $e_{\text{flux}} = (H - H_0) / H_0$, where $H_0 = (\sigma / 4\pi) T_{\text{eff}}^4$ is the net flux. For the models presented in Figure 4, e_{grad} is very small, typically 10^{-10} or less. The conservation of the total net flux is much harder to achieve; the bifurcated models have typically $e_{\text{flux}} \approx \text{few} \times 10^{-4}$ near the surface, while e_{flux} reaches a

few $\times 10^{-2}$ for column mass around $m \approx 10^2 \text{ g cm}^{-2}$ (that is, a few per cent), and drops to less than 10^{-5} at $m \approx 10^4 \text{ g cm}^{-2}$ and deeper. The error in the net total flux of several per cent might seem large, but one has to bear in mind that the net flux is a subtraction of two large quantities, $H^{\text{out}} - H^{\text{in}}$, and the actual numerical error $(H^{\text{out}} - H^{\text{in}} - H_0)/H^{\text{out}}$ is of the order of 10^{-5} or less. A dramatic demonstration of this fact is that a model, which is almost converged (maximum relative change in T and ρ was less than 10^{-3}), exhibits a seemingly ridiculous value of $e_{\text{flux}} \approx 10^5$ at upper layers $m < 10^2 \text{ g cm}^{-2}$ (i.e. an error in the total net flux of some $10^7\%$!), yet the actual temperature difference between this and the fully converged model is at most about 2-3 K, and the predicted flux in both cases is completely indistinguishable on a plot! This again shows that in the case of strong irradiation it is the value of $(H^{\text{out}} - H^{\text{in}} - H_0)/H^{\text{out}}$ (or e_{grad}) which is critical for practical convergence, not a much more stringent criterion of the error in the total net flux, e_{flux} .

The difference in the temperature structure is of course reflected in the emergent spectrum. In Figure 5 we show the emergent flux corresponding to the two solutions of the intermediate-irradiation (distance 0.08 AU) model, computed with TiO/VO. The models differ dramatically in the optical and in near-IR region because of the dramatically different surface temperature and the corresponding increase of the TiO/VO opacity. Since the low-surface- T branch exhibits a higher temperature at the plateau (see Fig. 4), the flux at the low-opacity regions is higher.

Finally, Fig. 6 displays the emergent flux for the two models for the highest irradiation, namely for the distance 0.0225 AU, which corresponds to OGLE-TR-56. The thick line is a model without TiO/VO, and the thin line with TiO/VO. There is no bifurcation here since both opacity tables led to unique solutions, however quite different ones. The corresponding spectra are thus significantly different as well.

5. Discussion and Conclusions

We have demonstrated that under certain circumstances the differences between the absorption mean and the Planck mean opacities can lead to multiple solutions for the atmospheric structure. This result is quite robust, and in fact represents a so far overlooked general result of elementary stellar atmospheres theory. Since we do not expect that the absorption and Planck mean opacities will differ significantly in the usual case of radiative equilibrium of non-irradiated atmospheres, the most interesting situations where the effect may play role are strongly irradiated stars and planets, and also, possibly, structures where there is a significant deposition of mechanical energy, such as stellar chromospheres and accretion disks. We are not concerned with these objects here, but would like to stimulate

further study of possible bifurcations for these situations. We note that Nolan & Lunine (1988) also found a bimodal behavior of the atmosphere of Triton which is linked to external irradiation.

From the physical point of view we may interpret the absorption mean opacity as the global absorption efficiency, and the Planck mean opacity as the global emission efficiency, of the medium. The integrated mean intensity J acts as a total absorption pool, while the integrated Planck function B as a total thermal pool. The radiative equilibrium, that stipulates that the total radiation energy absorbed on the spot is equal to the total energy emitted on the same spot, therefore acts as a thermostat: The radiative equilibrium sets the local temperature in such a way that $\kappa_J J = \kappa_B B$. Here J is determined by the radiative transfer, and the local temperature follows as $B \equiv (\sigma/\pi)T^4 = (\kappa_J/\kappa_B) J$. In the case of strong irradiation, the weighting that determines κ_J is dominated by the incoming radiation. If the monochromatic opacity in the region around the peak of the external irradiation is very sensitive to temperature, for instance if it is very high for high temperatures and very low for low temperatures, the “radiative-equilibrium thermostat” may find two solutions – either a high T together with high κ_J , or a low T with low κ_J ; in both cases the radiative equilibrium $\kappa_J J = \kappa_B B$ is satisfied.

However, the applicability of this effect to real objects depends critically on a degree of reliability of adopted opacities. For high-temperature conditions where the gaseous opacities dominate, the situation is relatively well under control, thanks to recent enormous progress in computing atomic data (Opacity Project, Iron Project, OPAL, and others; for a recent review see, e.g., Nahar 2003).

In the case of irradiated giant planets or other substellar-mass objects like L and T dwarfs, the opacity for low density ($\rho \approx 10^{-12} - 10^{-9} \text{ g cm}^{-3}$) and high temperature ($T > 2000 \text{ K}$) is still relatively uncertain. At the present stage, we cannot be sure that the bifurcation effect really occurs, but we have shown that this is certainly a very real possibility which should be taken into account when constructing atmospheric models.

The authors are pleased to thank Bill Hubbard, Thierry Lanz, Jonathan Lunine, Jim Liebert, Christopher Sharp, and Drew Milsom for fruitful conversations and help during the course of this work, as well as NASA for its financial support via grants NAG5-10760 and NAG5-10629. We also thank anonymous referee for a number of comments and suggestions.

REFERENCES

- Allard, F., Hauschildt, P.H., and Schwenke, D. 2000, *ApJ*, 540, 1005
- Borysow, A. and Frommhold, L. 1990, *ApJ*, 348, L41
- Borysow, A., Jørgensen, U.G., and Zheng, C. 1997, *A&A*, 324, 185
- Borysow, A. 2002, *A&A*, 390, 779
- Borysow, A., Champion, J.P., Jørgensen, U.G., Wenger, C. 2003, in *Stellar Atmospheric Modeling*, Eds. I. Hubeny, D. Mihalas, K. Werner, ASP Conf. Ser. 288, 651
- Burrows, A., Marley, M.S., and Sharp, C.M. 2000, *ApJ*, 531, 438
- Burrows, A., Ram, R.S., Bernath, P., Sharp, C.M., and Milsom, J.A. 2002, *ApJ*, 577, 986
- Burrows, A., & Sharp, C.M. 1999, *ApJ*, 512, 843
- Dimitrijević, M.S. and Peach, G. 1990, *A&A*, 236, 261
- Dulick, M., Bauschlicher, C. Jr., Burrows, A., Sharp, C.M., Ram, R.S., and Bernath, P. 2003, accepted to *ApJSuppl.*
- Goorvitch, D., 1994, *ApJS*, 95, 535
- Hubeny, I. 1988, *Comp. Phys. Commun.* 52, 103
- Hubeny, I. 1990, *ApJ*, 351, 632
- Hubeny, I., & Lanz, T. 1995, *ApJ*, 439, 875
- Hummer, D.G. 1982, *ApJ*, 257, 724
- Husson, N., Bonnet, B., Scott, N.A., and Chedin, A. 1994, *J. Quant. Spect. Rad. Transfer*, 48, 509
- Karkoschka, E., 1994, *Icarus*, 11, 174
- Konacki, M., Torres, G., Jha, S., & Sasselov, D.D. 2003, *Nature*, 421, 507
- Kurucz, R. L. 1994, *Atomic Data for Fe and Ni*, Kurucz CD-ROM 22 (Cambridge, Mass: SAO)
- Lodders, K., & Fegley, B. 2002, *Icarus*, 155, 393

- Mihalas, D. 1978, *Stellar Atmospheres*, 2nd Ed., (San Francisco: Freeman)
- Nahar, S. N. 2003, in *Stellar Atmospheric Modeling*, Eds. I. Hubeny, D. Mihalas, K. Werner, ASP Conf. Ser. 288, 651
- Nefedov, A.P., Sinel'shchikov, V.A., and Usachev, A.D. 1999, *Physica Scripta*, 59, 432
- Nolan, M.C., & Lunine, J.I. 1988, *Geophys. Res. Lett.* 15, 1315
- Partridge, H. and Schwenke, D.W. 1997, *J. Chem. Phys.*, 106, 4618
- Piskunov, N.E., Kupka, F., Ryabchikova, T.A., Weiss, W.W., and Jeffery, C.S. 1995, *ÅSuppl.*, 112, 525
- Plez, B., 1999, private communication.
- Rothman, L.S., Gamache, R.R., Tipping, R.H., Rinsland, C.P., Smith, M.A.H., Benner, D.C., Malathy Devi, V., Flaud, J.-M., Camy-Peyret, C., Perrin, A., Goldman, A., Massie, S.T., Brown, L.R., and Toth, R.A., 1992, *J. Quant. Spect. Rad. Transfer*, 48, 469
- Rothman, L.S. *et al.* 1998, *J. Quant. Spect. Rad. Transfer*, 60, 665
- Sasselow, D.D. 2003, *ApJ* (in press)
- Strong, K., Taylor, F.W., Calcutt, S.B., Remedios, J.J., and Ballard, J. 1993, *J. Quant. Spect. Rad. Transfer*, 50, 363
- Sudarsky, D., Burrows, A., & Hubeny, I. 2003, *ApJ*, 588, 1121
- Tyuterev, V.I., Babikov, Yu.L., Tashkun, S.A., Perevalov, V.I., Nikitin, A., Champion, J.-P., Wegner, Ch., Pierre, C., Pierre, G., Hilico, J.-C., and Loete, M. 1994, *J. Quant. Spect. Rad. Transfer*, 52, 459
- Zheng, C. and Borysow, A. 1995, *Icarus*, 113, 84

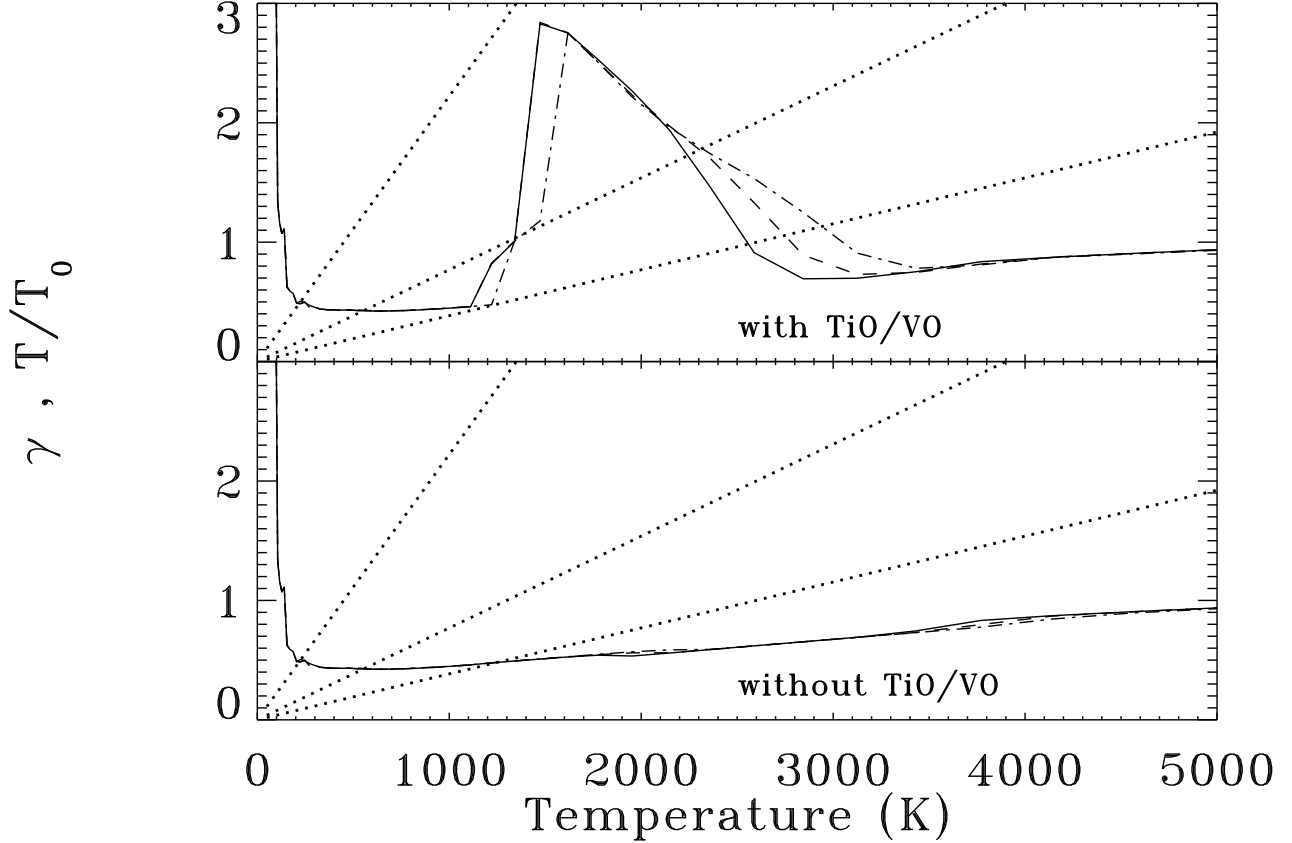


Fig. 1.— Opacity ratio index $\gamma = (\kappa_J/\kappa_B)^{1/4}$ plotted as a function of temperature. The upper panel shows the results for the opacities including TiO/VO, while the lower panel shows those without TiO/VO. The absorption mean opacity was evaluated using equation (23) with the stellar effective temperature $T_* = 6000$ K. The full line corresponds to a density ρ of 10^{-12} g cm $^{-3}$; the dashed line to $\rho = 10^{-11}$ g cm $^{-3}$; and the dot-dashed line to $\rho = 10^{-10}$ g cm $^{-3}$. The dotted lines represent the quantity T/T_0 , with T_0 corresponding to three different distances from the star. From top to bottom, $T_0 = 450$ K, (0.65 AU), $T_0 = 1250$ K (0.08 AU), and $T_0 = 2600$ K, (0.0225 AU). The intersections of the individual dotted lines with the $\gamma(T)$ curve represent possible solutions for the temperature in the upper layers of an irradiated atmosphere. In the case of the opacity table with TiO/VO, there are unique solutions for low and for high irradiation (corresponding to $T \approx 250$ K and $T \approx 2600 - 3000$ K), while in the intermediate cases there are indeed multiple solutions. The opacity table without TiO/VO does not exhibit a peak around 1500 K, so one obtains unique solutions for the temperature for all irradiations.

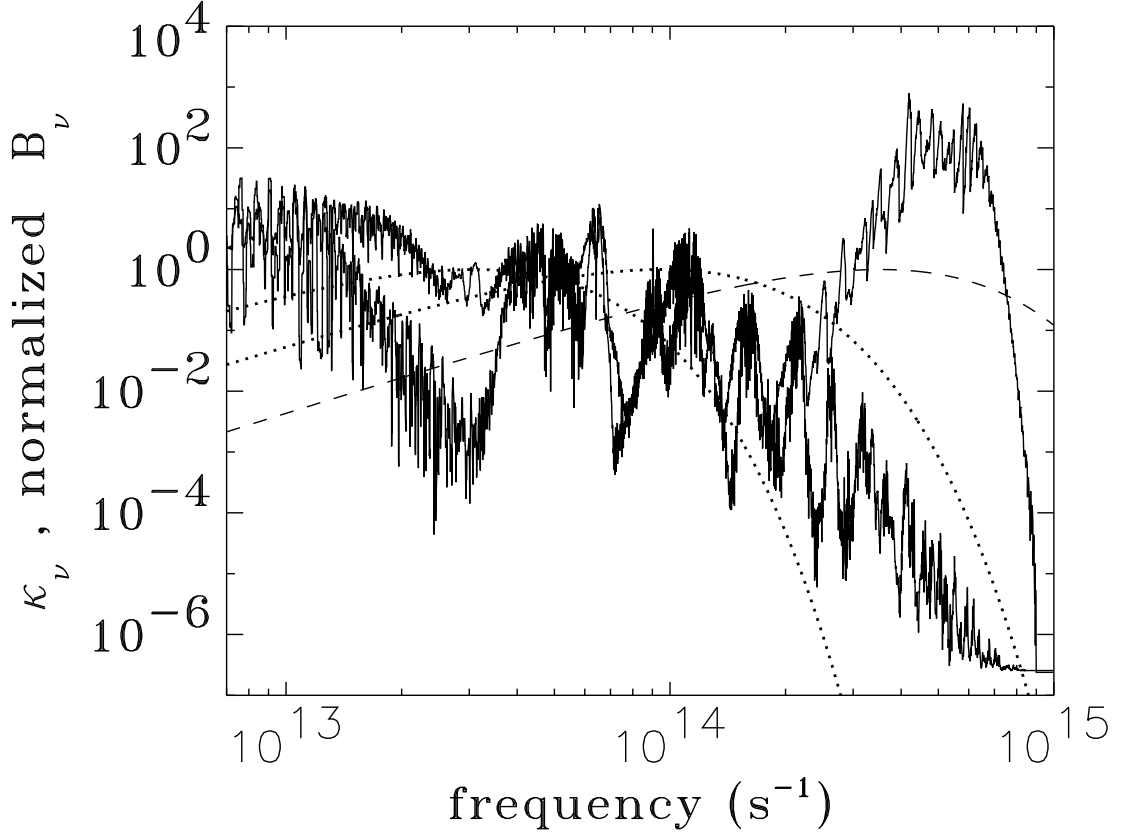


Fig. 2.— Monochromatic opacity (in $\text{cm}^2 \text{g}^{-1}$) as a function of frequency for density $\rho = 10^{-11} \text{g cm}^{-3}$ and for two temperatures, $T = 1600 \text{ K}$ (solid line, with a maximum around $\nu \approx 3 - 6 \times 10^{14} \text{ Hz}$), and $T = 520 \text{ K}$ (bold solid line); together with normalized Planck functions for $T = T_*$ (dashed line), and for the two nominal temperatures (1600 and 520 K – dotted lines). A large monochromatic opacity for $T = 1600 \text{ K}$ in the optical region where $B_\nu(T = T_*)$ has a maximum explains why $\kappa_J > \kappa_B$ for this temperature.

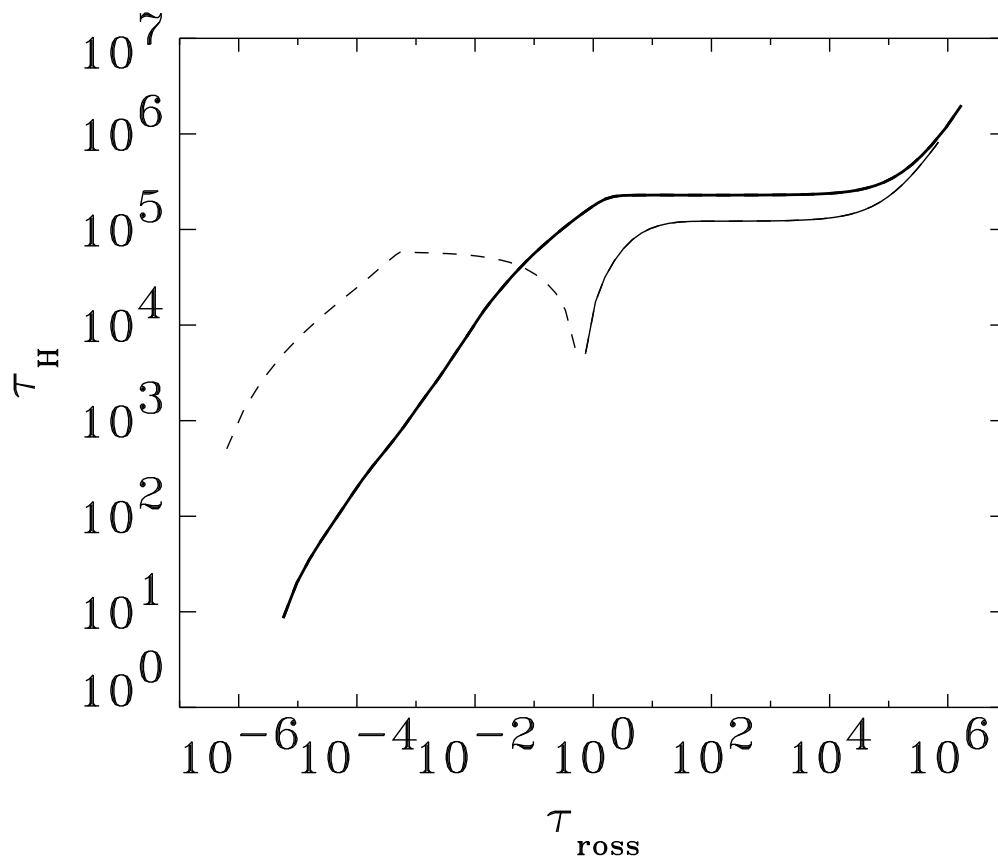


Fig. 3.— Flux-mean optical depth as a function of Rosseland mean optical depth for the two solutions of the intermediate-irradiation (distance 0.08 AU) model, computed with the TiO/VO opacity. The heavy line represents the low-surface- T branch; the thin line the high-surface- T branch. The solid line represents the positive values of τ_H , while the dashed line the negative values.

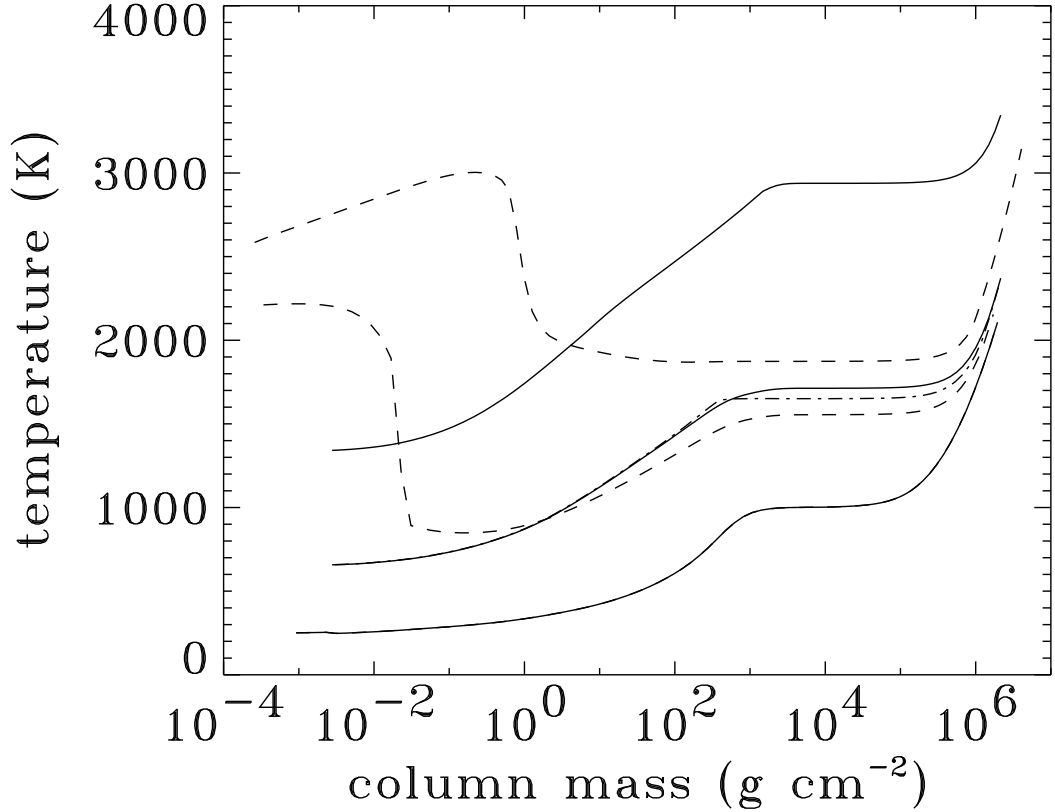


Fig. 4.— Temperature as a function of column mass. Solid lines represent models computed for the opacity table without TiO/VO, while the dashed and dot-dashed lines represent models with TiO/VO. The curves represent, from top to bottom, three distances from the central star. The top lines corresponds to 0.0225 AU, the middle lines to 0.08 AU, and the bottom lines to 0.65 AU. Numerical values of the dilution factor are $W = 2.8 \times 10^{-2}$, 2.2×10^{-3} , and 3.5×10^{-5} . The models for the lowest irradiation ($W = 3.5 \times 10^{-5}$) computed with and without TiO/VO are not distinguishable on the plot. The middle dashed and the dot-dashed lines represent the two solutions for the same distance, and thus illustrate the bifurcation discussed in the text.

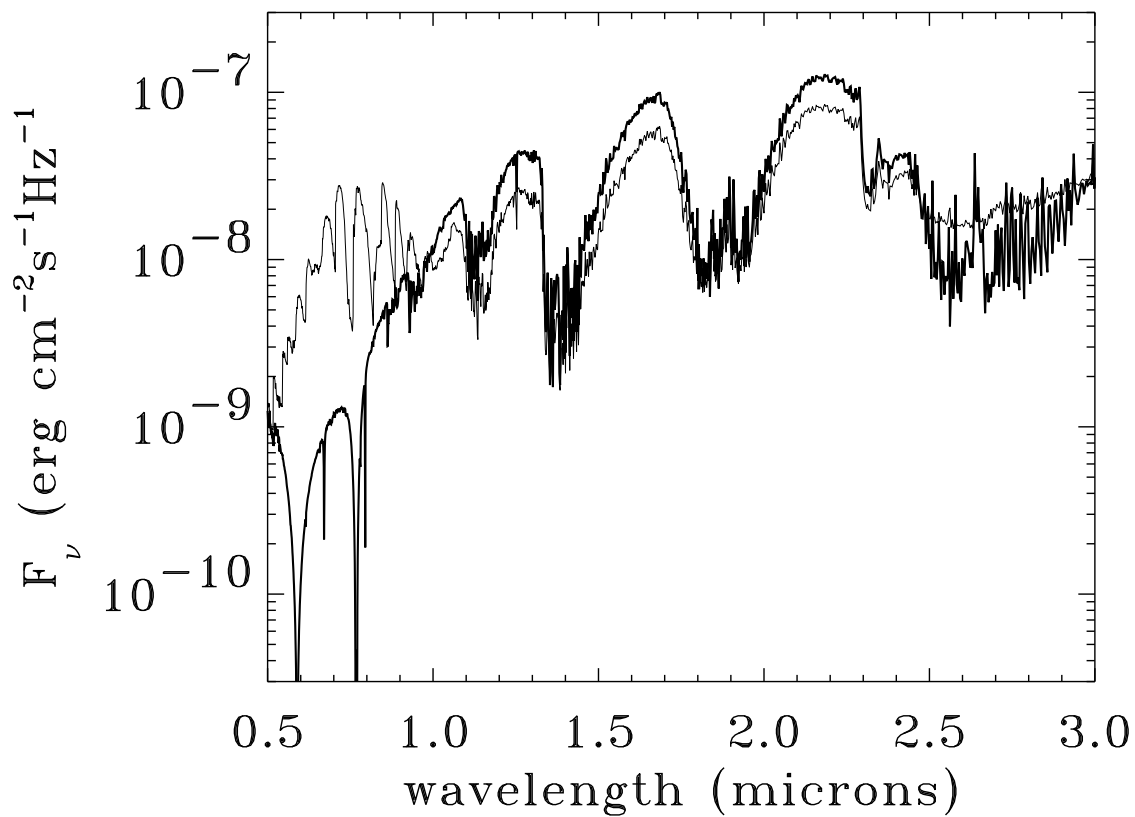


Fig. 5.— Emergent flux of a function of wavelength for the two solutions of the intermediate-irradiation (distance 0.08 AU) model, computed with TiO/VO. Heavy line represents the low-surface- T branch; the thin line the high-surface- T branch. The model flux computed without TiO/VO is very close to the low-surface- T branch, and for clarity is not displayed.

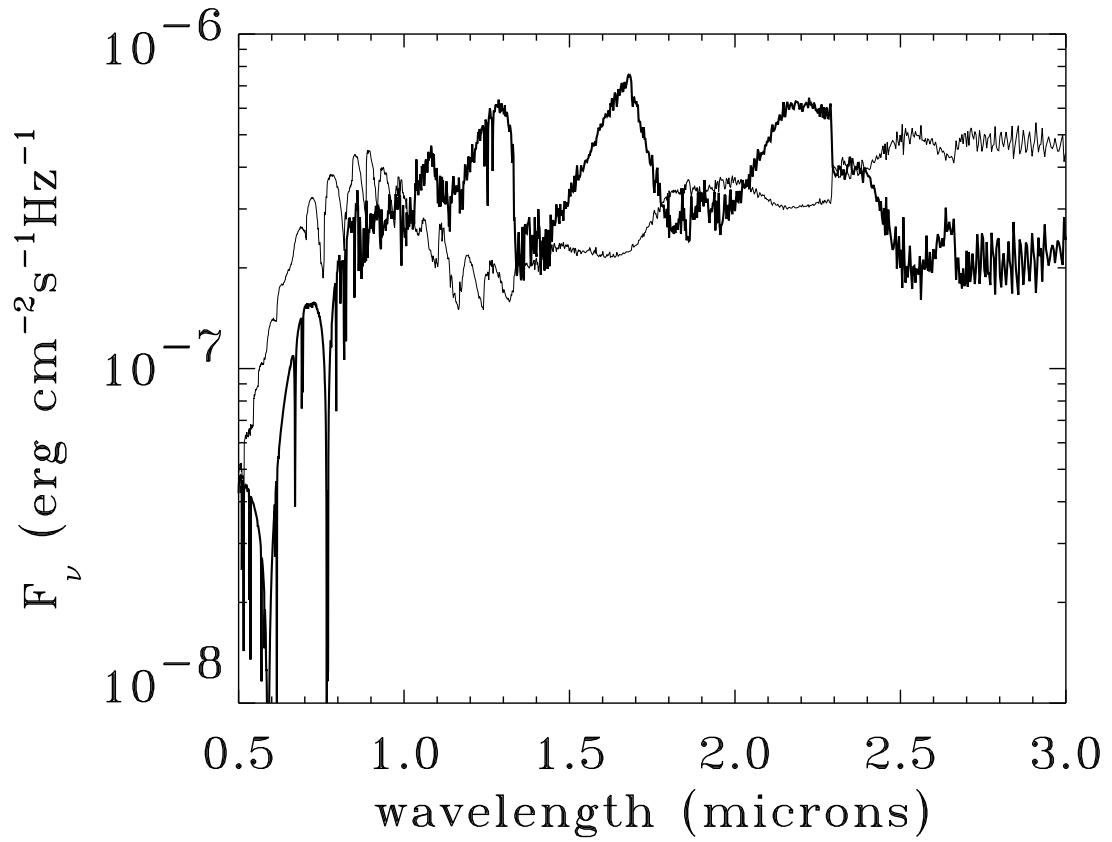


Fig. 6.— Emergent flux of a function of wavelength for the high-irradiation (distance 0.0225 AU) model, computed without TiO/VO (thick line) and with TiO/VO (thin line).